Bound-free electron-positron pair production in relativistic heavy-ion collisions

Helmar Meier, Zlatko Halabuka, Kai Hencken, and Dirk Trautmann
Institut für theoretische Physik der Universität Basel, Klingelbergstrasse 82, 4056 Basel, Switzerland

Gerhard Baur
Institut für Kernphysik (Theorie), Forschungszentrum Jülich, 52425 Jülich, Germany
(Received 15 August 2000; published 13 February 2001)

We study the bound-free electron-positron pair production in relativistic heavy-ion collisions to different bound states in a full plane-wave Born approximation calculation. Exact Dirac wave functions are used for both the bound electron and the free positron in the final states. Results for the relativistic heavy-ion collider as well as the forthcoming large hadron collider are given. This process is one of the dominant beam loss processes and can become critical for the operation with heavy ions. A simple parametrization is given as well. We compare our results with calculations of other groups.

DOI: 10.1103/PhysRevA.63.032713 PACS number(s): 34.50.−s, 25.75.−q, 12.20.−m

I. INTRODUCTION

Bound-free pair production is one of the new types of processes that occurs in relativistic collisions of atoms and ions. It is the production of an electron-positron pair with the electron not produced as a free state, but as a bound state of one of the ions:

$$Z_P + Z_T \rightarrow Z_P + (Z_T + e^-) + e^+. \tag{1}$$

This process changes the charge state of the ion. Due to the change in the charge-to-mass ratio, such an ion will be lost from the circulating beam and the luminosity will be seriously affected. Together with the electromagnetic dissociation, this process is the dominant beam loss process at the relativistic heavy-ion collider (RHIC) and the large hadron collider (LHC) at CERN when using heavy ions [1–3]. In addition to the beam loss itself, it was recently discussed in [4] that the capture process can lead to localized beam-pipe heating. This could cause magnet quenches if the local cooling is inadequate. Therefore, it is very important to know this cross section with high accuracy and reliability.

We want to mention also that the corresponding process using antiprotons as the ‘‘target’’ has recently found an application in the production and detection of relativistic antihydrogen; see [5,6]. In a collision of the antiprotons with a target, again electron-positron pairs are produced. The positron can be produced in a bound state of the antiproton forming an antihydrogen atom. Using the equivalent photon method, this cross section was calculated in [7]. In the equivalent photon approximation, the cross section factorizes into a photoinduced cross section and an equivalent photon spectrum. This spectrum depends on a cutoff parameter, which should be chosen appropriately. Using the plane-wave Born approximation (PWBA) expression for the cross section, one can avoid this ambiguity and see also how this parameter should be chosen. This was done in [8] and [9]. In these papers, differential as well as total cross sections are given as a function of the collisional energy. Whereas in the latter reference, approximate lepton wave functions appropriate for low values of Z_T, the charge of the antiproton, have been used, exact Dirac wave functions, which are also valid for higher values of Z_T, have been used in [8].

It is the purpose of this paper to calculate the cross sections for the energy region of the colliders RHIC and LHC exactly within the plane-wave Born approximation or (which is equivalent) the semiclassical straight line approximation (SCA), including also higher shells. Previously, such kinds of calculations were done using the Weizsäcker-Williams method [10,11]. Higher-order effects (in the interaction with the projectile) have been considered by a number of groups, see, for example, [12–14]. Recently, exact calculations have been done in the high-energy limit by Baltz [15]. He finds that the contributions from higher orders are rather small (of the 1% level) and even tend to decrease the cross section. This is in contrast to results found at much smaller energies with Lorentz factors in the target rest frame $\gamma_T < 3$ [16,17], but see also [18,19].

In Sec. II we extend the formalism presented in [8] to the relativistic heavy-ion case, also including now formulaes for the higher atomic states. Numerical results are then presented in Sec. III and we discuss the dependence on the beam energy and on the principle quantum numbers n and κ. We review these results with those existing in the literature in Sec. IV. Finally, our conclusions are given in Sec. V.

II. PWBA OR SCA THEORY OF BOUND-FREE PAIR PRODUCTION

The total cross section for bound-free pair production (per electron state) in Lorentz gauge is given by [20,8]

$$\sigma_{n_f,\kappa_f}^{(bfpp)} = 8\pi\left(\frac{Z_P\alpha_{em}}{\beta_T}\right)^2 \times \sum_{\kappa_i} \int_m^\infty dE_i \int_{k_z}^\infty \frac{dk \quad F(k^2-\beta_T^2 k_z^2)}{k^3[1-(\beta_T k_z/k)^2]^2} \times \sum_{m_f m_i} |\langle \psi_f(\vec{r})|(1-\vec{\beta}_T\cdot\vec{\alpha})e^{i\vec{k}\cdot\vec{r}}|\psi_i(\vec{r})\rangle|^2, \tag{2}$$

where $\vec{\beta}_T=\vec{v}/c$ is the velocity of the projectile in the target rest frame, $\gamma_T=(1-\beta_T^2)^{-1/2}$ is the Lorentz factor in the target rest frame, and $F(k^2)$ is the form factor of the charge distribution of the projectile. For electrons and positrons, we can set this form factor $F(k^2)\equiv 1$. (For the pair production of muons and tauons, this form factor will become important.) We denote the fine-structure constant by α_{em} to distinguish it from the usual Dirac matrices $\vec{\alpha}$. The spatial momentum transfer from projectile to target is $\hbar\vec{k}$. The absolute value of the wave vector $\vec{k}$ is denoted by k, and its z component is related to the energy of the photon as

$$k_z=\frac{\omega}{v}=\frac{E_f-E_i}{\hbar v}. \tag{3}$$

The total energy of the bound electron is E_f and the one of the electron in the continuum is E_i. (Please note that E_i is negative.) $\psi_i(\vec{r})$ and $\psi_f(\vec{r})$ are the Dirac-Coulomb wave functions describing the initial negative continuum state and final bound state. The charge numbers of the projectile and target are denoted by Z_P and Z_T.

The same expression Eq. (2) in the Coulomb gauge reads

$$\sigma_{n_f,\kappa_f}^{(bfpp)}=8\pi\left(\frac{Z_P\alpha_{em}}{\beta_T}\right)^2 \times\sum_{\kappa_i}\int_m^\infty dE_i\int_{k_z}^\infty\frac{dk}{k^3}F(k^2-\beta_T^2k_z^2) \times\sum_{m_fm_i}\left|\langle\psi_f(\vec{r})|\left(1-\frac{\vec{\beta}_{T\perp}\cdot\vec{\alpha}}{1-(\beta_Tk_z/k)^2}\right)e^{i\vec{k}\cdot\vec{r}}|\psi_i(\vec{r})\rangle\right|^2. \tag{4}$$

Equation (4) can be obtained from Eq. (2) by making use of the current conservation. Both equations are therefore identical only when exact eigenfunctions of the Dirac Hamiltonian are used, as already stressed in [20,21].

The four-component Dirac spinor in a spherically symmetric field is given by

$$\psi_\kappa^m=\begin{pmatrix} g_\kappa(r)\chi_\kappa^m(\hat{r})\\ if_\kappa(r)\chi_\kappa^m(\hat{r})\end{pmatrix}. \tag{5}$$

The angular dependence is expressed by the spin-angular functions

$$\chi_\kappa^m(\hat{r})=\sum_{\tau=\pm 1/2}(-1)^{l+m-1/2}\sqrt{2j+1} \times\begin{pmatrix} l & \frac{1}{2} & j\\ m-\tau & \tau & -m\end{pmatrix}Y_l^{m-\tau}(\hat{r})\chi_\tau, \tag{6}$$

where χ_τ is the Pauli spinor and

$$j=|\kappa|-\frac{1}{2},\quad l=j+\frac{1}{2}\,\mathrm{sgn}(\kappa). \tag{7}$$

The radial Dirac equation is

$$\frac{dg}{dr}=-\frac{\kappa+1}{r}g+\frac{mc}{\hbar}\left[1+\frac{E-V(r)}{mc^2}\right]f, \tag{8}$$

$$\frac{df}{dr}=\frac{\kappa-1}{r}f+\frac{mc}{\hbar}\left[1-\frac{E-V(r)}{mc^2}\right]g. \tag{9}$$

The radial functions in the Coulomb field $V(r)=-\zeta/r$ (with $\zeta=\alpha_{em}Z_T$) for the bound states are given by

$$\begin{pmatrix} g_{n,\kappa}(r)\\ f_{n,\kappa}(r)\end{pmatrix}=N[mc^2\pm\sqrt{(mc^2)^2-(\hbar c\beta)^2}]^{1/2}(\beta r)^{\gamma-1} \times e^{-\beta r}\left[\pm\left(\frac{\zeta mc^2}{\hbar c\beta}-\kappa\right)\mathrm{F}(-n_r,2\gamma+1;2\beta r) -n_r\,\mathrm{F}(1-n_r,2\gamma+1;2\beta r)\right]. \tag{10}$$

The corresponding energy eigenvalues are

$$E_{nj}=mc^2\left[1+\frac{\zeta^2}{(n-j-\frac{1}{2}+\gamma)^2}\right]^{-1/2}, \tag{11}$$

where n is the principle quantum number defined by

$$n=n_r+|\kappa|. \tag{12}$$

The quantity β corresponding to the energy eigenvalue is

$$\beta=\frac{mc}{\hbar}\frac{\zeta}{[(n_r+\gamma)^2+\zeta^2]^{1/2}}. \tag{13}$$

γ is given by

$$\gamma=\sqrt{\kappa^2-\zeta^2}. \tag{14}$$

The adequate normalization for bound states is

$$\int d^3r\,\psi^\dagger(\vec{r})\psi(\vec{r})=\int_0^\infty drr^2[g^2(r)+f^2(r)]=1 \tag{15}$$

and the normalization constant is found to be

$$N=\frac{2^\gamma\beta^2}{\Gamma(2\gamma+1)}\left[\frac{\Gamma(2\gamma+n_r+1)}{2mc^2(n_r!)\frac{\zeta mc^2}{\hbar c}\left(\frac{\zeta mc^2}{\hbar c\beta}-\kappa\right)}\right]^{1/2}. \tag{16}$$

The continuum Dirac-Coulomb wave functions are

$$\begin{pmatrix} g_{E,\kappa}(r) \\ f_{E,\kappa}(r) \end{pmatrix} = \left(\frac{E+mc^2}{E-mc^2}\right)^{1/4} \frac{k'}{(\pi\hbar c)^{1/2}} N_f(k'r)^{\gamma-1} \times \begin{pmatrix} \mathrm{Re} \\ \mathrm{sgn}(E)\sqrt{\dfrac{E-mc^2}{E+mc^2}} \quad \mathrm{Im} \end{pmatrix} \times [e^{-i(k'r+\varphi)}{}_1\mathrm{F}_1(\gamma+i\eta, 2\gamma+1, 2ik'r)], \tag{17}$$

which are normalized according to

$$\int_0^\infty dr r^2 [g_{E,\kappa} g_{E',\kappa} + f_{E,\kappa} f_{E',\kappa}] = \delta(E-E'). \tag{18}$$

In Eq. (17) k', η, φ, and N_f are given by

$$k' = \frac{\sqrt{E^2-(mc^2)^2}}{\hbar c}, \quad \eta = \frac{\zeta E}{\hbar c k'},$$

$$e^{2i\varphi} = \frac{-\kappa + i\eta \dfrac{mc^2}{E}}{\gamma - i\eta}, \tag{19}$$

$$N_f = \frac{2^\gamma e^{\pi\eta/2} |\Gamma(\gamma+1+i\eta)|}{\Gamma(2\gamma+1)}. \tag{20}$$

Please note that $E > mc^2$ for positive-energy continuum wave functions and $E < -mc^2$ for negative-energy states.

Starting from the expression in the Coulomb gauge (4), the angular integration can be performed analytically [22] to get

$$\sigma^{(bfpp)}_{n_f,\kappa_f} = 32\pi^2 \left(\frac{Z_P \alpha_{em}}{\beta_T}\right)^2 \sum_{\kappa_i} \int_m^\infty dE_i \int_{k_z}^\infty \frac{dk}{k^3} \times \left\{ T_l + \frac{\beta_T^2}{2} \frac{1}{[1-(\beta_T k_z/k)^2]^2} \left(1 - \frac{k_z^2}{k^2}\right) T_\perp \right\}. \tag{21}$$

This equation can be rewritten as an integration over $k_\perp$, with $k^2 = k_\perp^2 + k_z^2$:

$$\sigma^{(bfpp)}_{n_f,\kappa_f} = 16\pi^2 \left(\frac{Z_P \alpha_{em}}{\beta_T}\right)^2 \sum_{\kappa_i} \int_m^\infty dE_i \int_0^\infty \frac{d(k_\perp^2)}{k_\perp^2 + k_z^2} \times \left\{ \frac{1}{k_\perp^2 + k_z^2} T_l + \frac{\beta_T^2}{2} \frac{k_\perp^2}{[k_\perp^2 + (k_z/\gamma_T)^2]^2} T_\perp \right\}. \tag{22}$$

In this form the increase of the cross section with $\ln \gamma_T$ can be clearly seen due to the second term (proportional to $T_\perp$) in the integral. T_l and $T_\perp$ are given by

$$T_l = \frac{(2j_f+1)(2j_i+1)}{4\pi} \times \sum_l (2l+1) \frac{1}{2} [1 + (-1)^{l_f+l+l_i}] |J^l(k)|^2 \times \begin{pmatrix} j_f & l & j_i \\ \frac{1}{2} & 0 & -\frac{1}{2} \end{pmatrix}^2, \tag{23}$$

$$\begin{aligned} T_\perp = \frac{(2j_f+1)(2j_i+1)}{4\pi} &\times \sum_l (2l+1) \left\{ \frac{1}{2}[1+(-1)^{l_f+l+l_i+1}] \frac{1}{l(l+1)} \right. \\ &\times |(\kappa_i+\kappa_f) I_l^+(k)|^2 + \frac{1}{2}[1+(-1)^{l_f+l+l_i}] \frac{1}{(2l+1)^2} \\ &\times \left| \left(\frac{l+1}{l}\right)^{1/2} [(\kappa_i-\kappa_f) I_{l-1}^+(k) - l I_{l-1}^-(k)] \right. \\ &\left.\left. - \left(\frac{l}{l+1}\right)^{1/2} [(\kappa_i-\kappa_f) I_{l+1}^+(k) + (l+1) I_{l+1}^-(k)] \right|^2 \right\} \\ &\times \begin{pmatrix} j_f & l & j_i \\ \frac{1}{2} & 0 & -\frac{1}{2} \end{pmatrix}^2, \end{aligned} \tag{24}$$

and the radial integrals are

$$J^l(k) = \int_0^\infty dr r^2 j_l(kr) [g_{E_i,\kappa_i}(r) g_{n_f,\kappa_f}(r) + f_{E_i,\kappa_i}(r) f_{n_f,\kappa_f}(r)], \tag{25}$$

$$I_l^\pm(k) = \int_0^\infty dr r^2 j_l(kr) [g_{E_i,\kappa_i}(r) f_{n_f,\kappa_f}(r) \pm f_{E_i,\kappa_i}(r) g_{n_f,\kappa_f}(r)]. \tag{26}$$

These rapidly oscillating radial integrals are in general very difficult to calculate. T_l and $T_\perp$ are independent of the Lorentz factor γ and can be evaluated before the integration over k and E_i in Eq. (21). Also, the summation over the κ_i can be done in advance. Results for different values of γ can then be obtained from the same set of T_l and $T_\perp$. We were able to do the evaluation of the radial integrals in Eqs. (25) and (26), using the recursion relations from [23]. These relations are rather stable in the whole range studied by us. As individual terms can become quite large or small, we were forced to use floating point numbers with an extended range of the exponent. The convergence of the sum, on the other hand, was no problem. We have also independently checked the accuracy of the radial integrals by a direct integration. For the very high values of γ we are interested in, the integration extends to both the very low and the very high values

TABLE I. Cross section for the bound-free pair production of *one* ion *only* for different bound states are given for RHIC and LHC conditions for different ion-ion collisions. Also given are the parameters A and B to be used in Eq. (28) for the dependence on the Lorentz factor γ_c.

Bound state	σ(RHIC) (b)	σ(LHC) (b)	A (b)	B (b)
^{1}H-^{1}H	$\gamma_c=250$	$\gamma_c=7500$		
1s	2.62×10^{-11}	4.25×10^{-11}	5.36×10^{-12}	-3.40×10^{-12}
2s	3.28×10^{-12}	5.31×10^{-12}	6.70×10^{-13}	-4.23×10^{-13}
2p(1/2)	3.75×10^{-17}	6.10×10^{-17}	7.73×10^{-18}	-5.20×10^{-18}
2p(3/2)	1.47×10^{-17}	2.41×10^{-17}	3.10×10^{-18}	-2.42×10^{-18}
3s	9.70×10^{-13}	1.57×10^{-12}	1.98×10^{-13}	-1.26×10^{-13}
^{20}Ca-^{20}Ca	$\gamma_c=125$	$\gamma_c=3750$		
1s	1.61×10^{-2}	2.92×10^{-2}	3.84×10^{-3}	-2.48×10^{-3}
2s	2.00×10^{-3}	3.62×10^{-3}	4.78×10^{-4}	-3.07×10^{-4}
2p(1/2)	1.39×10^{-5}	2.52×10^{-5}	3.35×10^{-6}	-2.33×10^{-6}
2p(3/2)	3.63×10^{-6}	6.70×10^{-6}	9.02×10^{-7}	-7.27×10^{-7}
3s	5.90×10^{-4}	1.07×10^{-3}	1.41×10^{-4}	-9.10×10^{-5}
^{47}Ag-^{47}Ag	$\gamma_c=109$	$\gamma_c=3264$		
1s	3.51	6.46	8.68×10^{-1}	-5.63×10^{-1}
2s	4.33×10^{-1}	7.98×10^{-1}	1.07×10^{-1}	-6.94×10^{-2}
2p(1/2)	2.81×10^{-2}	5.21×10^{-2}	7.05×10^{-3}	-5.02×10^{-3}
2p(3/2)	3.80×10^{-3}	7.16×10^{-3}	9.87×10^{-4}	-8.31×10^{-4}
3s	1.26×10^{-1}	2.34×10^{-1}	3.13×10^{-2}	-2.02×10^{-2}
^{79}Au-^{79}Au	$\gamma_c=100$	$\gamma_c=3008$		
1s	94.9	176	23.8	-14.7
2s	12.1	22.4	3.04	-1.87
2p(1/2)	3.62	6.77	9.27×10^{-1}	-6.56×10^{-1}
2p(3/2)	2.10×10^{-1}	4.01×10^{-1}	5.62×10^{-2}	-4.93×10^{-2}
3s	3.46	6.40	8.67×10^{-1}	-5.34×10^{-1}
^{82}Pb-^{82}Pb	$\gamma_c=99$	$\gamma_c=2957$		
1s	121	225	30.4	-18.7
2s	15.5	28.8	3.91	-2.39
2p(1/2)	5.21	9.76	1.34	-9.46×10^{-1}
2p(3/2)	2.78×10^{-1}	5.33×10^{-1}	7.50×10^{-2}	-6.61×10^{-2}
3s	4.42	8.20	1.11	-6.79×10^{-1}
^{92}U-^{92}U	$\gamma_c=97$	$\gamma_c=2900$		
1s	263	488	66.0	-39.0
2s	34.4	63.7	8.63	-5.10
2p(1/2)	16.7	31.3	4.30	-3.00
2p(3/2)	6.77×10^{-1}	1.30	1.83×10^{-1}	-1.63×10^{-1}
3s	9.67	17.9	2.43	-1.44

of k, as well as E_i. We have therefore used a logarithmic grid using values for E_i and k up to $500m_e$. Up to 200 angular momenta l (and therefore also κ) were used to get a good convergence. The final integration over E_i and k was then done with an automatic integration with high accuracy. The routine was especially sensitive to the peaked nature of the integral at $E_i\sim k$. Up to the values of γ of the LHC, which we were interested in, we expect the overall accuracy of the final cross section to be about 1%.

III. NUMERICAL RESULTS

We give our results for symmetrical collisions where the charges of both ions are equal; $Z_P=Z_T=Z$. The cross sections refer to capture to *one* of the ions *only*. Since the cross section for capture scales with Z_P^2, the cross section for asymmetrical collisions is obtained by scaling the cross sections with Z_P^2/Z^2.

In Table I we give the cross sections for the different ions and for different bound states. This table was already presented in [22,24]. We have used the conditions as they are relevant for Au-Au at RHIC and Pb-Pb at LHC. In these colliders, each of the ions is assumed to have a Lorentz factor of $\gamma_c=Z/A\gamma_p$. For RHIC we take $\gamma_p=250$; for LHC $\gamma_p=7500$, respectively. For different values of γ_c the cross section can be obtained by using Eq. (28). The cross sections are larger than the ones quoted in the ''ALICE technical report'' [3]. The Lorentz factor γ_T in the rest frame of one of

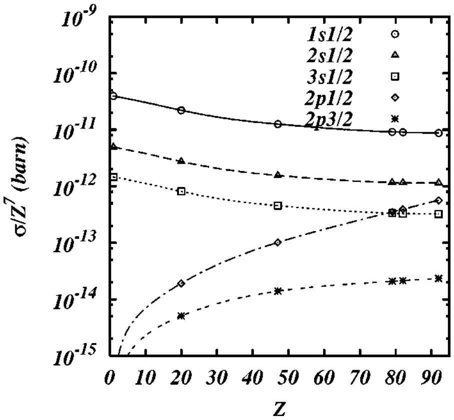

FIG. 1. The cross section for the capture of the electron into different bound states is given as a function of the charge of the ion charge Z. A Lorentz factor in the c.m. system of $\gamma_c = 3400$, corresponding to an equivalent Lorentz factor of $\gamma_T = 2.3\times 10^7$ in the rest frame of the ion is used. For s states there is an approximate Z^7 scaling of the cross section.

the ions, which is the relevant one for the bound-free pair production, is then given by

$$\gamma_T = 2\gamma_c^2 - 1. \tag{27}$$

For RHIC (LHC) this corresponds to $\gamma_T = 2\times 10^4$ ($\gamma_T = 1.8\times 10^7$). For large values of γ_c it was found that the cross sections can be parametrized as [13]

$$\sigma = A\ln(\gamma_c) + B. \tag{28}$$

We also give the values of the constants A and B in the table.

In Fig. 1 we show the dependence of the different cross sections on the ion charge Z. As the cross section for the s states is known to be proportional to Z^7 for low values of Z [25], we divide through this factor. The most striking result is that the cross section for the capture into the $2p_{1/2}$ state increases rapidly with Z and becomes even larger than the one for the $3s$ state for heavy ions. The cross section for the $2p_{3/2}$ shows a clearly different behavior. We attribute this difference to the "small component" of the Dirac wave function. This wave function has an s-wave character for the $p_{1/2}$ state and a d-wave character for the $p_{3/2}$ state, respectively. With the increase of Z, the "small component" gets more important and leads to the different behavior of the two cross sections. This is also in accord with a qualitative discussion of relativistic effects of the Dirac wave function for bound states as a function of Z [26].

For the cross section to the different s states as a function of the principle quantum number n, a scaling law is found in the nonrelativistic limit,

$$\sigma_{ns} = \frac{\sigma_{1s}}{n^3}, \tag{29}$$

that also appears, e.g., in the photoelectric effect [26]. This scaling law arises because the value of the wave function at the origin,

$$\sigma \sim |\psi(0)|^2, \tag{30}$$

enters in the expression for the cross section. Our calculations confirm this $1/n^3$ scaling to a high accuracy once more and for all values of Z. With this scaling law we can sum the contribution from capture processes into all s states [25],

$$\sum_{n=1}^{\infty} \sigma_{ns} = \zeta(3)\sigma_{1s} \approx 1.202\sigma_{1s}, \tag{31}$$

where ζ denotes the Riemann ζ function. For low atomic numbers Z the contributions from s orbits are the most important ones, whereas the cross section to the $2p_{1/2}$ contributes of the order of 6.5% in the heaviest cases.

IV. COMPARISON WITH OTHER CALCULATIONS

In this section we want to give a comparison of the results that have been obtained with different approaches. The results for the cross section are summarized in Table II. A large number of calculations exist, including the electromagnetic interaction (with the projectile) to all orders. Most of

TABLE II. Cross section for bound-free pair production of *one* ion *only* into the $1s$-state calculated by different groups are compared. The last entry uses experimental results of bound-free pair production into any bound state at CERN SPS with 158 GeV/A energies. Given are the results for Au-Au collisions at RHIC and Pb-Pb collisions at LHC. For details of the different calculations see the text.

σ(Au-Au,RHIC, $\gamma_c = 100$) (b)	σ(Pb-Pb,LHC, $\gamma_c = 2957$) (b)	Ref.
94.9	225	This work
93	226	[27,14]
37	86	[25]
89	206 (from U)	[12,13,18]
	195 (from Au)	
72		[30]
90	222 ($\gamma_c = 3400$)	[10]
77 ($b_{min} = 2\lambda_c$)		[11]
85 ($b_{min} = \lambda_c$)		
94	204 b	[38]

them have been done for beam energies much smaller than those available at the relativistic heavy-ion colliders. In order to get results for energies, at RHIC and especially at LHC energies extrapolations were used; see below.

A calculation within the PWBA approximation was done by Becker and co-workers [27,28,14]. Calculations up to values of $\gamma_T = 1000$ have been done and an interpolation formula of the form

$$\sigma \approx Z_P^2 Z_T^5 a \ln(\gamma_T/\gamma_0) \tag{32}$$

(using our notation) and tabulated values for a and γ_0 can be found in [27]. The parameters a and γ_0 depend slightly on Z_T. Using the value of a for $Z=80$ for both Au and Pb, we get values of 93 b (Au-Au at RHIC) and 226 b (Pb-Pb at LHC), respectively.

In [25] a calculation is done making use of the Sommerfeld-Maue wave functions as an approximation to the exact Coulomb-Dirac continuum wave functions and also using an approximation for the bound-state wave function, which is valid in the limit $Z\alpha \ll 1$. They found their result in SCA to be equal to the one derived within the equivalent photon approximation. Using their formula we obtain results that are substantially lower (by a factor of 2) than our results here. As their approximation is strictly valid only in the limit $Z\alpha \ll 1$, such a discrepancy is perhaps not surprising.

Baltz *et al.* treated the problem in a series of papers [12,13,18,29]. For large impact parameter they also make use of a perturbative treatment. In addition, they simplify the interaction potential by taking only lowest-order terms in $1/\gamma_T$ and also expanding in ρ/b, where ρ is the electron coordinate and b the impact parameter. They proposed the parametrization of the cross section for large values of γ_T of the form

$$\sigma = A \ln(\gamma_T) + B, \tag{33}$$

with the interpretation of A to be given by the perturbative part only and the influence of higher-order terms at small impact parameter to be present in B only (of course this parametrization is identical to the one of Becker *et al.* above). Tabulated values for A and B are given in [13]. From them (and choosing for $b_{min} = 1\lambda_c$), we get a cross section of 83 b (Au-Au at RHIC), 161 b (Au-Au at LHC), and 436 b (U-U at LHC). They also give the cross section to be 89 b (Au-Au at RHIC) in the text where contributions from non-perturbative processes at small impact parameter have been included. No results for lead-lead collisions are given, but assuming a Z^7 scaling, we get (from the extrapolation of the Au results) a value of 206 b (Pb-Pb at LHC), and from the extrapolation of the U results, a value of 195 b (Pb-Pb at LHC) using the γ_T dependence of Eq. (33).

In [30] a calculation is done using the cross section of the free pair production cross section and folding it with the momentum distribution of the bound state. The electron is therefore described by a plane wave. For Au-Au collisions at RHIC, a cross section of 72 b was found by them, but see also [31].

Two calculations making use of the equivalent photon approximations have been performed also. In both, exact solutions of the Dirac equations are used. In the equivalent photon method, a cutoff parameter has to be introduced, which leads to some uncertainty in the results. In [10] capture to the 1s state was calculated. The results were also compared with the cross section for bound-free pair production induced by real photons at low photon energies by [32]. For the heavy-ion case, values of 90 b (Au-Au at RHIC) and 222 b (Pb-Pb at LHC, $\gamma_c = 3400$) are given, respectively. Also tabulated values of A and B are presented. Their results are in good agreement with the present values. The cutoff parameter was taken to be the Compton wavelength of the electron. In [11] similar calculations are performed also including capture cross-section calculations to the L shell. Agreement with the results of [10] was found for the K shell. A critical discussion of the use of the cutoff parameter present in the equivalent photon spectrum was done. The exact value of this parameter is not given by the Weizsäcker-Williams theory and therefore introduces some uncertainties in the results. For Au-U collisions at RHIC with the electron being captured by the U atom, they find a value of 165 b for $b_{min} = 2\lambda_c$ and 182 b for $b_{min} = \lambda_c$, with λ_c the Compton wavelength of the electron. Comparing these results with the 195 b we get, a cutoff parameter of $b_{min} = \lambda_c$ seems to be favored. Again, assuming a scaling of the result with Z_T^5, we get for Au-Au collisions at RHIC 77 b ($b_{min} = 2\lambda_c$) and 85 b ($b_{min} = \lambda_c$), respectively. Unfortunately no results for LHC energies are given.

Experiments were first done at Bevalac at 1 GeV/A [33–35]. A cross section of 2.19(0.25) b for Au-U collisions and capture on the U projectile was found. Experiments were also done at the alternating-gradient synchroton at 10.8 GeV/A corresponding to $\gamma_T = 12.6$, $\gamma_c = 2.6$ [36,37]. A cross section of 8.8 b was found for Au-Au collisions (our calculation gives 11.86 b.[1] The experimental results were found to be in agreement with the theoretical results of [28,30].)

A measurement has recently been done at the CERN SPS with a 158 GeV/A Pb beam ($\gamma_T \approx 168$, corresponding to $\gamma_c = 9.2$) [38]; see also [39]. The capture to the Pb ion was studied for several different targets. For a gold target, a value of 44.3 b is given (our result is 45 b). Assuming a scaling of the cross section as given above Eq. (28) and assuming $B = -24$ b from [18], they give extrapolated values of 94 b (Au at RHIC) and 204 b (Pb at LHC). Again, these values agree quite well with our results.

V. CONCLUSIONS AND OUTLOOK

Apart from neglecting higher-order effects in the projectile charge, we have given a full calculation of the bound-free capture cross section. Since such higher-order effects were shown to be small [15], our predictions should be very reliable. Overall our results are in agreement with a number of other calculations, using different approaches. These calculations are also very important for the questions of lumi-

[1]Please note that while we compare cross sections for the 1s state only in comparison with other calculations, comparing with experimental results we use the total cross section into all bound states.

nosity loss and localized beam pipe heating [4], especially at the LHC.

Muon and τ-lepton bound-free pair production can be calculated similarly. Since the bound-free pair-production cross section scales with $1/m_{lepton}^2$ [25], these cross sections will be much smaller than the ones for e^+-e^- pair production. Especially for heavy nuclei, it will be necessary to use finite-size lepton wave functions. In addition to the $1/m_{lepton}^2$ scaling, there will also be a severe reduction of the cross section due to the form-factor effects. Maybe such exotic atoms could be interesting for physics [40]. We mention that the lifetime of the free τ lepton is given by $ct = 87.2\mu$. For a Lorentz factor of about 100, this is still a very short distance of about 0.1 mm for the decay length of such an atom. On the other hand, a muonic atom lives long enough and could be extracted from the beam (similar to the antihydrogen experiments [5,6]).

In a fixed target experiment, the effect of screening the atomic electrons can be incorporated as well by using a screened Coulomb potential for both the wave function, as well as the interaction with the projectile [$F \not\equiv 1$ in Eq. (2)]. This could be relevant for the CERN fixed target experiments [38,39]. This effect has been studied in [41] and was found to be on the percent level.

RHIC is running right now and we expect that the present numbers will soon be tested. In the meantime an article by Bertulani and Dolci appeared [42]. This is a continuation of [9] to the heavy-ion case. In it they give an explanation why the approximation used in [25] does not work well for large values of Z.

ACKNOWLEDGMENTS

We would like to thank Daniel Brandt and Spencer Klein for very interesting and useful comments and discussions, which helped us also in order to make this work clearer.

[1] Conceptual design of the relativistic heavy-ion collider, Brookhaven National Laboratory Report No. BNL52195, 1989.
[2] D. Brandt, K. Eggert, and A. Morsch, Transparencies of the ALICE workshop, Report No. CERN AT/94-05, 1994.
[3] N. Ahmad *et al.*, Alice Technical Proposal No. CERN/LHCC 95-71, 1995.
[4] S. R. Klein, Lawrence Berkeley National Laboratory Report No. LBNL-45566, e-print physics/0005032 (unpublished).
[5] G. Baur *et al.*, Phys. Lett. B **368**, 251 (1996).
[6] G. Blanford *et al.*, Phys. Rev. Lett. **80**, 3037 (1998).
[7] C. T. Munger, S. J. Brodsky, and I. Schmidt, Phys. Rev. D **49**, 3228 (1994).
[8] H. Meier *et al.*, Eur. Phys. J. C **5**, 287 (1998).
[9] C. A. Bertulani and G. Baur, Phys. Rev. D **58**, 034005 (1998).
[10] A. Aste, K. Hencken, D. Trautmann, and G. Baur, Phys. Rev. A **50**, 3980 (1994).
[11] C. K. Agger and A. H. Sørensen, Phys. Rev. A **55**, 402 (1997).
[12] A. J. Baltz, M. J. Rhoades-Brown, and J. Weneser, Phys. Rev. A **44**, 5569 (1991).
[13] A. J. Baltz, M. J. Rhoades-Brown, and J. Weneser, Phys. Rev. A **48**, 2002 (1993).
[14] U. Becker, J. Phys. B **20**, 6563 (1987).
[15] A. J. Baltz, Phys. Rev. Lett. **78**, 1231 (1997).
[16] K. Momberger, N. Grün, and W. Scheid, Z. Phys. D: At., Mol. Clusters **18**, 133 (1991).
[17] K. Rumrich, G. Soff, and W. Greiner, Phys. Rev. A **47**, 215 (1993).
[18] A. J. Baltz, M. J. Rhoades-Brown, and J. Weneser, Phys. Rev. A **50**, 4842 (1994).
[19] K. Momberger, A. Belkacem, and A. H. Sørensen, Europhys. Lett. **32**, 401 (1995).
[20] J. Eichler and W. E. Meyerhof, *Relativistic Atomic Collisions* (Academic Press, San Diego, 1995).
[21] J. Eichler, Phys. Rep. **193**, 165 (1990).
[22] H. Meier, Ph.D. thesis, Universität Basel, 1999.
[23] D. Trautmann, G. Baur, and F. Rösel, J. Phys. B **16**, 3005 (1983).
[24] H. Meier *et al.*, Annual Report 1999, Institut für Kernphysik, Forschungszentrum Jülich, Juel-3744, 1999, ISSN0944-2952.
[25] C. A. Bertulani and G. Baur, Phys. Rep. **163**, 299 (1988).
[26] H. A. Bethe and E. E. Salpeter, *Quantum Mechanics of One- and Two-Electron Atoms* (Springer Verlag, Berlin, 1957).
[27] R. Anholt and U. Becker, Phys. Rev. A **36**, 4628 (1987).
[28] U. Becker, N. Grün, and W. Scheid, J. Phys. B **20**, 2075 (1987).
[29] A. J. Baltz, M. J. Rhoades-Brown, and J. Weneser, Phys. Rev. E **54**, 4233 (1996).
[30] M. J. Rhoades-Brown, C. Bottcher, and M. R. Strayer, Phys. Rev. A **40**, 2831 (1989).
[31] G. Baur, Phys. Rev. A **44**, 4767 (1991).
[32] W. R. Johnson, D. J. Buss, and C. O. Carroll, Phys. Rev. **5**, A1232 (1964).
[33] A. Belkacem, H. Gould, B. Feinberg, R. Bossingham, and W. E. Meyerhof, Phys. Rev. Lett. **71**, 1514 (1993).
[34] A. Belkacem, H. Gould, B. Feinberg, R. Bossingham, and W. E. Meyerhof, Phys. Rev. Lett. **73**, 2432 (1994).
[35] A. Belkacem, H. Gould, B. Feinberg, R. Bossingham, and W. E. Meyerhof, Phys. Rev. A **56**, 2806 (1997).
[36] N. Claytor, A. Belkacem, T. Dinneen, B. Feinberg, and H. Gould, Phys. Rev. A **55**, R842 (1997).
[37] A. Belkacem, N. Claytor, T. Dinneen, B. Feinberg, and H. Gould, Phys. Rev. A **58**, 1253 (1998).
[38] P. Grafström *et al.*, CERN Report No. CERN/SL-99-033 EA, 1999.
[39] H. F. Krause *et al.*, Phys. Rev. Lett. **80**, 1190 (1998).
[40] M. S. Weiss, in *Phase Space Approach to Nuclear Dynamics*, Trieste, Italy, 1985, edited by M. di Toro *et al.* (World Scientific, Singapore, 1985).
[41] A. B. Voitkiv, N. Grün, and W. Scheid, Phys. Lett. A **269**, 325 (2000).
[42] C. Bertulani and D. Dolci, e-print nucl-th/0008015, 2000.